applied sciences

MDPI

Article

Optimization in the Absorption and Desorption of CO_2 Using Sodium Glycinate Solution

Pao Chi Chen * and Sheng-Zhong Lin

Department of Chemical and Materials Engineering, Lunghwa University of Science and Technology, Taoyuan City 33306, Taiwan; yh6081414@gmail.com

* Correspondence: chenpc@mail2000.com.tw

Received: 27 July 2018; Accepted: 18 October 2018; Published: 24 October 2018

Abstract: This study used sodium glycinate as an absorbent to absorb CO_2 in the bubble column scrubber under constant pH and temperature environments to obtain the operating range, CO_2 loading, and mass transfer coefficient. For efficient experimentation, the Taguchi method is used for the experimental design. The process parameters are the pH, gas flow rate (Q_g), liquid temperature (T), and absorbent concentration (C_L). The effects of the parameters on the absorption efficiency, absorption rate, overall mass transfer coefficient, gas–liquid molar flow rate ratio, CO_2 loading, and absorption factor are to be explored. The optimum operating conditions and the order of parameter importance are obtained using the signal/noise (S/N) ratio analysis, and the optimum operating conditions are further verified. The verification of the optimum values was also carried out. The order of parameter importance is pH > C_L > Q_g > T. Evidence in the ^{13}CNMR (Carbon 13 Nuclear Magnetic Resonance) spectra shows that the pH value has an effect on the solution composition, which affects both the absorption efficiency and mass transfer coefficient. There are 18 experiments for regeneration, where the operating temperature is 100–120 °C. The heat of regeneration was measured according to the thermodynamic data. The CO_2 loading, the overall mass transfer, and the heats of regeneration correlation are also discussed in this work. Finally, an operating policy for the CO_2 absorption process was confirmed.

Keywords: sodium glycinate; bubble column; Taguchi method; absorption

1. Introduction

Global warming is a critical issue in the world. Because of this, the Paris Agreement declared that the global mean temperature increment must not exceed 2 °C by 2100, and aims to reduce the temperature to 1.5 °C. This shows that the reduction of greenhouse gas is more pressing [1–3]. Fossil fuels are the most significant factors in the warming process, and the energy, petrochemical, steel, transportation, and cement industries are the major contributors. Electricity is mainly derived from thermal power plants, and the thermal power plants burn fossil fuels, where CO_2 is the main source of the greenhouse effect.

Nowadays, there are three common systems for capturing CO_2, including post-combustion, pre-combustion, and oxyfuel-combustion. In a post-combustion system, the CO_2 concentration is 3–15% [4], which is mostly removed by chemical absorption. The common solvents for chemical solvent absorption processes include amines, NaOH, aqueous ammonia, ionic liquids, hot potassium carbonate, and amino acid salt. Among these solvents, the amine is studied a lot. Monoethanolamine (MEA) is universally used as an absorbent by over a thousand commercial plants, because it has a high absorption rate, high alkalinity, regenerability, and low price, but the it also has low loading, deterioration, high corrosively, and a high regenerated energy [3]. In order to improve the absorption and stripping efficiency, it is imperative to find new, more efficient solvents, such as

methyldiethanolamine (MDEA), diethanolamine (DEA), diethylenetriamie (DETA), piperazine (PZ), ionic liquids, and blended amines [5–11]. Compared with MEA, it has been found that regeneration energy can be largely reduced for both single amines and blended amines [9,12].

Industrially, the chemical solvent absorption process is used for capturing CO_2. The CO_2 absorption and stripping double unit operating system is usually used [13–17]. The cost of the CO_2 post-combustion capture would increase the cost of electricity production by 70%. Therefore, improving the efficiency of absorbent, environmental factors and regeneration efficiency are the key points of subsequent studies [15–17]. This includes operating range and loading control for scrubber and reboiler temperature and flow rate for stripper.

Therefore, the studies using amino acid salt as an absorbent have been noted by scholars. In order to improve on the drawback of alkanolamines, including their oxidative degredation and high vapor pressure resulting in solvent loss and degradation product handling, many alternative solvents have been tested [3,6–11,18–22], in which amino acid salts are found to be more attractive solvents. This is because amino acid salt solutions have a better resistance to degradation, have a negligible volatility, and no environmental issue [23]. Because of this, using amino acid salt solutions as solvents capturing CO_2 have been carried out in various modes; Kumar et al. [24], Portugal et al. [25], Lee et al. [26], Park et al. [18], and Vaidya et al. [21] have all studied the absorption kinetics of CO_2 using aqueous amino acid salts, while the thermodynamic properties of amino acid salt solutions have been explored by Park et al. [27], Song et al. [28], Salazar et al. [29], and Shaikh et al. [30]. Amino acid salt has the aforesaid characteristics, but there will be precipitates in some concentration conditions, blocking the absorption plant pipeline. Therefore, the concentration must be controlled when the amino acid salt is used to capture CO_2.

However, the reaction mechanism after CO_2 absorption is similar to that of amines, as follows:

$$^{-}OOC - R - NH_2 + CO_2(g) \rightleftarrows {}^{-}OOC - R - NHCOO^{-} + H^{+} \quad (1)$$

$$CO_2(aq) + OH^{-} \rightleftarrows HCO_3^{-} \rightleftarrows CO_3^{2-} + H^{+} \quad (2)$$

$$^{-}OOC - R - NHCOO^{-} + H_2O_2 \rightleftarrows HCO_3{}^{-} + {}^{-}OOC - R - NH_2 \quad (3)$$

$$^{-}OOC - R - NH_2 + H^{+} \rightleftarrows {}^{-}OOC - R - NH_3{}^{+} \quad (4)$$

$$H_2O \rightleftarrows H^{+} + OH^{-} \quad (5)$$

In Equations (1)–(5), it can be found that the pH of the solution has an effect on the absorption and the distribution of the species. Increasing the pH means decreasing the $[H^+]$, which favors a forward reaction in Equation (1), and hence favors CO_2 absorption. On the other hand, it favors the formation of $HCO_3{}^{-}$, $^{-}OOC - R - NHCOO^{-}$, and $^{-}OOC - R - NH_2$. Aqueous amino acid salt, which is similar to that of aqueous amino acid zwitterion, will be protonated or deprotonated by changing the pH, as shown in reaction [18], as follows:

$$^{+}NH_3 - R - CO_2H \overset{pK_1}{\rightleftarrows} {}^{+}NH_3 - R - CO_2{}^{-} \overset{pK_2}{\rightleftarrows} NH_2 - R - CO_2{}^{-} \quad (6)$$

It can be found that a low pH ($pH < pK_1$) amino acid salt represents positive charges, $HOOC - R - NH_3^{+}$. In the range of pK_1 and pK_2, the medium pH range becomes the zwitterion form, $^{-}OOC - R - NH_3^{+}$. At a low pH value, the reaction of amino acid with CO_2 is less. Thus, knowing how to control the pH, temperature, and flow rate in order to obtain the desired absorption rate, efficiency, and mass transfer coefficient becomes significant. This can be achieved by adding an amino acid salt solution into the scrubber, which can maintain the desired pH to a certain value, where CO_2 can be effectively captured.

In addition, the selection of the scrubber is also significant, as it affects the performance of the CO_2 absorption. Here, the bubble-column has been used, as it shows a superior performance, such as

a high absorption, high mass-transfer coefficient, simple structure, and easy operation, compared with other scrubbers [2]. However, some parameters, such as the gas-flow rate, liquid-flow rate, solution temperature, and the pH of the solution have been found to be key factors affecting the absorption of CO_2. Because of the importance of mass transfer in a bubble-column, some papers have studied the effects of the process parameters on the mass transfer coefficients [31–36]. The reported values were in the range of 0.01–0.888, depending on the conditions. A comparison of their mass transfer coefficients is listed in Table 1. However, there are no available data in the literature regarding the absorption of CO_2 using a sodium glycinate solution. In addition, the effect of pH on the solution and operating range can be effectively explored using a bubble-column scrubber. Therefore, a study of the absorption and desorption of CO_2 using a sodium glycinate solution becomes significant.

Table 1. Mass transfer coefficient for various bubble-columns. MEA—monoethanolamine.

References	Mass Transfer Coefficient (s^{-1})	Conditions	Remarks
Vandu et al. [31]	0.02–0.14	Gas flow rate = 0–0.43.8 m/s Solvent: paraffin oil Slurry concentration (Al_2O_3): 0–0.25	Stripping of O_2 using N_2 in a slurry bubble column
Dhaouadi et al. [32]	0.01–0.20	Gas flow rate = 0.01–0.28 m/s T = 25 °C; Solvent: tap water Gas: N_2/Air	Absorption of O_2 using tap water
Lau et al. [33]	0.045–0.085	Gas flow rate = 3.2–10.8 m/s T = 25 °C; Solvent: tap water Gas: N_2/O_2	Absorption of O_2 using tap water
Al-Naimi et al. [34]	0.01–0.14	Gas flow rate = 0.02167–0.2068 m/s Solvent: tap water, glycerin, and alcohol Slurry concentration (PVC): 25–100 kg/m^3	Absorption of O_2 using tap water, glycerin, and alcohol solvents
Chen et al. [35]	0.0342–0.888	pH = 9.0–11; T = 25–45 °C; G = 4–9.5 L/min Solvent: 4M MEA CO_2 concentration:15–60%	Absorption of CO_2 using MEA solution
Chen et al. [36]	0.051–0.305	pH = 9.5–11.5; T = 25–60 °C; G = 3–5 L/min Solvent: aqueous ammonia (28%) CO_2 concentration:15–60%	Absorption of CO_2 using aqueous ammonia solution

2. Methodology

In order to reach their purpose, a mass transfer model accompanying a two-film model, thermodynamic data, and an energy duty model were used. The framework used in here is proposed in Figure 1. This study is divided into three parts, as follows: the first part uses sodium glycinate solution to capture CO_2. In order to explore the effects of the process variables on the absorption efficiency (E), absorption rate (R_A), overall mass transfer coefficient ($K_G a$), gas–liquid molar flow rate ratio (γ), absorption factor (φ), and CO_2 loading (α) in a steady state condition, a bubble-column scrubber was adopted to study the capture of CO_2 under a constant pH and constant solution temperature environments. The second part uses the Taguchi experimental design and Taguchi analysis to find the optimum operating conditions and the order of importance, which are validated further. In addition, two optimum operating conditions are used for the uncontrolled experiments. The third part uses the scrubbed liquids collected from optimum conditions for the regeneration experiments, so as to evaluate the energy duty of the sodium glycinate solution. Finally, the correlation equations were obtained for further discussion.

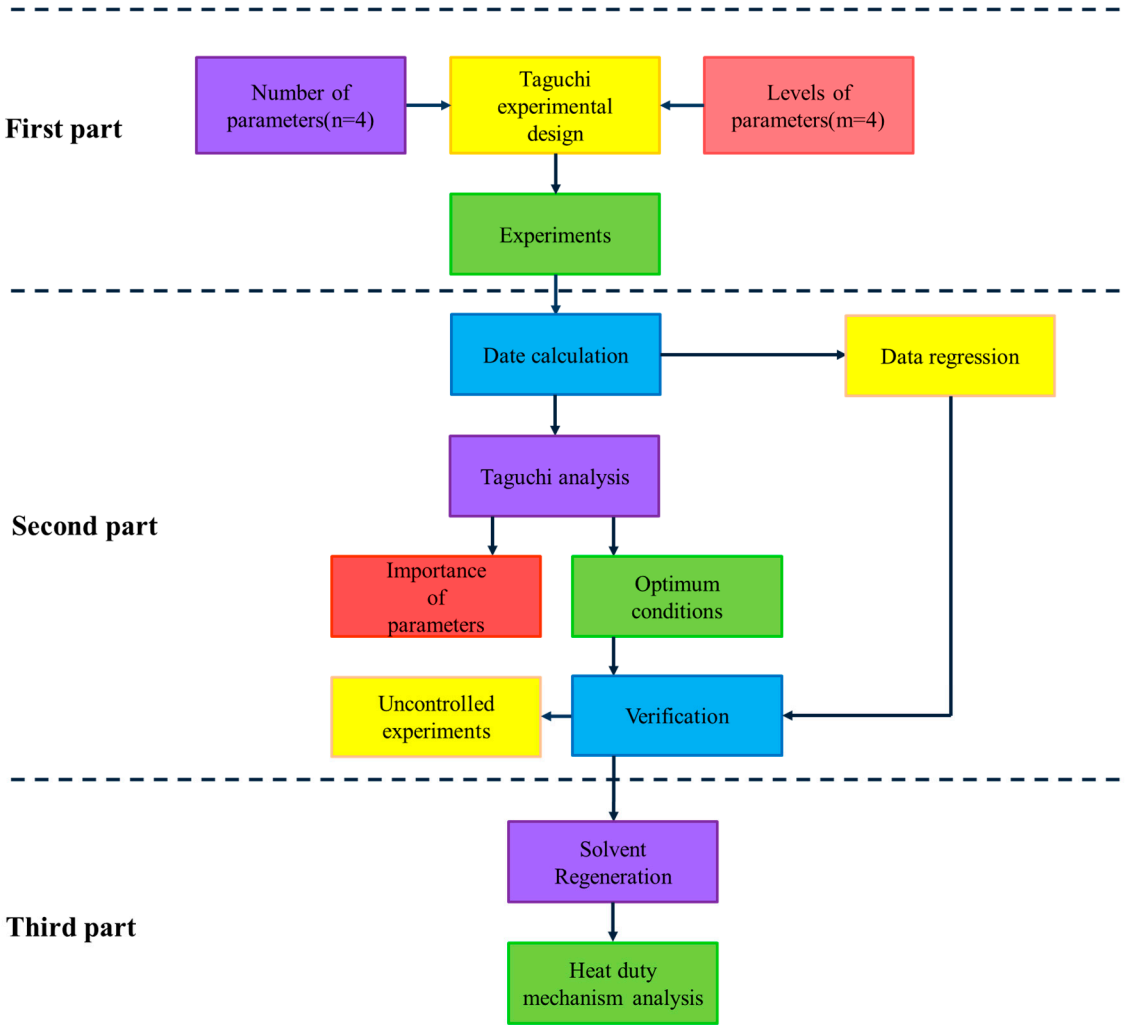

Figure 1. Concept of research framework used in this work.

2.1. Determinations of Experimental Data

2.1.1. Determination of R_A and K_Ga

In a bubble-column scrubber, a gas mixture containing CO_2 (A) and N_2 (B) flowing into a bubble column from the bottom comes into continuous contact with the liquid solvent flowing into the column from the top. The gas mixture and liquid simultaneously come into contact within the column counter. If a binary A–B system is assumed, then R_A and K_Ga can be obtained using the mass balance with two-film models at a steady-state condition [2]. Therefore, R_A can be written as follows:

$$R_A(\text{mols}^{-1}\text{L}^{-1}) = \frac{F_{A1}(\text{mol/s})}{V_L(\text{L})}[1 - (\frac{1 - y_{A1}}{y_{A1}})(\frac{y_{A2}}{1 - y_{A2}})] \quad (7)$$

where F_{A1} is the CO_2 gas molar flow rate, which can be evaluated when Q_g (gas flow rate), P_{A1} (partial pressure of CO_2 at inlet), and T (liquid temperature in the buble column) are available. In addition, V_L is the volume of liquid in the scrubber, y_{A1} is the CO_2 gas molar fraction at the inlet, and y_{A2} is the CO_2 gas molar fraction at the outlet. On the other hand, K_Ga becomes the following:

$$K_Ga(\text{s}^{-1}) = \frac{Q_g(\text{L/s})}{V_L(\text{L})} \ln \frac{F_{A1}(\text{mol/s})}{F_{A2}(\text{mol/s})} \quad (8)$$

Considering the ideal gas law for the inlet and outlet gases, F_{A1}/F_{A2} could be replaced with (P_1/P_2) (T_2/T_1) (y_{A1}/y_{A2}).

2.1.2. Determination of Gas–Liquid Flow Rate Ratio

Assuming that the input gas obeys the ideal gas law, the total gas flow rate can be calculated by Equation (9), as follows:

$$F_G(\text{mols}^{-1}) = Q_g(\text{L/s}) \times C_g(\text{mol/L}) = Q_g \frac{P_1(\text{atm})}{R(\text{atm} \times \text{LK}^{-1}\text{mol}^{-1})T(\text{K})} \quad (9)$$

where Q_g is the total gas volumetric flow rate and P_1 is the total pressure at the inlet. On the other hand, the liquid flow rate can be estimated by Equation (10), as follows:

$$F_L(\text{mols}^{-1}) = Q_L(\text{L/s}) \times C_L(\text{mol/L}) \quad (10)$$

where Q_L is the total liquid volumetric flow rate determined at a steady state condition and C_L is the concentration of sodium glycinate solution. Once F_G and F_L have been determined, γ can be obtained, as follows:

$$\gamma(\text{mol/mol}) = \frac{F_G(\text{mol/s})}{F_L(\text{mol/s})} \quad (11)$$

2.1.3. Determination of Scrubbing Factor

The scrubbing factor has been defined in a previous study [2], as shown below:

$$\phi(\text{molmol}^{-1}\text{L}^{-1}) = \gamma(\text{mol/mol}) \times \frac{E}{V(\text{L})} \times y_1 \quad (12)$$

where V is the volume of the scrubber. The scrubbing factor can be evaluated when γ, E, V, and y_1 are available.

2.2. Thermal Data Estimated

Heat duty of solvent regeneration includes three parts, as follows:

$$\begin{aligned} Q(\text{GJt}^{-1}) &= Q_{abs}(\text{GJ/t}) + Q_{sen}(\text{GJ/t}) + Q_{sol}(\text{GJ/t}) \\ &= \Delta H_{abs}(\text{GJ/t}) + \frac{m_{sol}(\text{kg})C_p(\text{kJkg}^{-1}\text{K}^{-1})\Delta T(\text{K}) \times 10^{-3}}{\Delta m_{CO_2}(\text{kg})} + \\ &\frac{1 \times 10^{-3}}{\Delta m_{CO_2}(\text{kg})/t_1(\text{s})} \left[\left(\frac{\Delta m_1(\text{kg})}{t_1(\text{s})} \times \Delta H_{vap}(\text{kJ/kg}) \right) - \dot{Q}_C(\text{kJ/s}) \right] \end{aligned} \quad (13)$$

They can be determined when the thermal data are available. The thermal data used here includes the heat capacity, heat of absorption, and latent heat, which have been reported in the literature, as shown in Table 2. In here, ΔH_{abs} is heat of absorption, which is related to loading α and temperature [22,29]. In addition, C_p is the heat capacity of the solvent, ΔT is the temperature difference, m_{sol} is the mass of regeneration solvent, Δm_{CO_2} is the mass loss of CO_2 after stripping. Here, C_p can be adopted, as shown in the literature [37], and can be correlated with the weight fraction and temperature. Finally, ΔH_{vap} is the heat of evaporation, $\dot{Q}_c$ is the cooling rate, Δm_1 is the solvent loss during stripping, and t is the evaporation time. By collecting the thermal data reported in the literature [27], ΔH_{vap} can be expressed as a function of the weight fraction (ω).

Table 2. Thermal data evaluated in the study.

Items	Parameters Related in Thermal Data Equations	Reference
ΔH_{abs}	T and α	[29]
C_P	T	[37]
ΔH_{vap}	ω	[27]

The three thermal data equations were shown below:

$$\Delta H_{abs}(\text{kJ/mol}) = 5.8048 \exp\left(\frac{583.84}{T(\text{K})}\right)\alpha^{0.5228} \tag{14}$$

$$C_P(\text{kJ/kg} \cdot \text{K}) = 3.1702 + 9.067 \times 10^{-4} T\,(\text{K}) \tag{15}$$

$$\Delta H_{vap}(\text{kJ/mol} \cdot \text{K}) = 4.244\omega^2 - 4.937\omega + 2.023 \tag{16}$$

2.3. Experimental

2.3.1. Experimental Design

Figure 1 shows the structure diagram of the Taguchi experimental design for the absorption and solvent regeneration studies. Three parts have been explored in the absorption study: the first is the Taguchi experiment, the second is the verification of the optimum conditions, and the third is the uncontrolled study. Finally, the solvent regeneration study is explored, using the solvents collected in the verification experiments as test solvents.

2.3.2. Experimental Design for Absorption Study

The first part of this study is CO_2 absorption. The process parameters used in here are the pH of the solution, gas flow rate (Q_g), liquid temperature (T), and solvent concentration (C_L), and each factor has four levels, as shown in Table 3. Theoretically, there should be $4^4 = 256$ experiments. Because of this, a Taguchi experimental design [16] was adopted, and the number of experiments was reduced to L_{16} (4^4) = 16; thus, we could save on the time and experimental cost. The signal/noise (S/N) ratio is calculated according to the larger-the-better value and smaller-the-better values from the data obtained in a steady state condition, expressed as Equations (17) and (18), respectively. The sequence of importance and optimum conditions are found using the S/N analysis. Where E, R_A, $K_G a$, and φ take the larger-the-better value, and γ takes the larger-the-better value and the smaller-the-better value, searching for the gas and liquid flow rate ratio range. Table 3 shows the factors and levels of the absorption experiment. Table 4 shows the orthogonal table for the absorption experiment.

$$\frac{S}{N} = -10 \times \log\left(\frac{1}{n}\sum_{1}^{n} z_i^2\right) \tag{17}$$

and

$$\frac{S}{N} = -10 \times \log\left(\frac{1}{n}\sum_{1}^{n} \frac{1}{z_i^2}\right) \tag{18}$$

where S/N is the objective function, n is the number of data, and z_i is the number of measures.

Table 3. Parameters and levels in the absorption study. Q_g—gas flow rate; C_L—solvent concentration.

Factor	1	2	3	4
(A) pH	9.5	10	10.5	11
(B) Q_g [L min^{-1}]	3	5	7	9
(C) T [°C]	25	30	35	40
(D) C_L [M]	3	4	5	6

Table 4. Orthogonal array in the absorption study.

No.	pH	Q_g	T	C_L
	(-)	(L min^{-1})	(°C)	(M)
1	9.5	3	25	3
2	9.5	5	30	4
3	9.5	7	35	5
4	9.5	9	40	6
5	10	3	30	5
6	10	5	25	6
7	10	7	40	3
8	10	9	35	4
9	10.5	3	35	6
10	10.5	5	40	5
11	10.5	7	25	4
12	10.5	9	30	3
13	11	3	40	4
14	11	5	35	3
15	11	7	30	6
16	11	9	25	5

2.3.3. Experimental Design for Solvent Regeneration

The second part of this study is the scrubbed solvent regeneration; this experimental procedure is similar to that reported in the literature [9,38]. The test solvents that were selected are from the optimum conditions obtained in here. A total of six solvents were adopted each for the three level temperatures (100 °C, 110 °C, and 120 °C).

2.4. Experimental Procedure

2.4.1. Absorption of CO_2

The equipment for the absorption experiment is shown in Figure 2, including the bubble column, cooling circulator, tubing pump, CO_2 detector, heater, mass flow controller, and pressure gauge. The sodium glycinate solution absorbs the CO_2 in the bubble column, under a constant pH environment, then the simulated flue gas concentration (15%) and temperature (50 °C) from the coal-fired power plant are pumped into the column. First, the absorbent concentration for the experiment is prepared—the CO_2 detector (Guardian Plus, D600, Hartford, CT, USA), pressure indicator (SR-321), pH controller (Suntex, PC-310, New Taipei City, Taiwan), and heating controller (5020 Data Acquisition System) are switched on; the mass flow controller (N_2 and CO_2) (Bronkhorst, F-201CB DMFC) is adjusted to the correct flow for the experiment; and the CO_2 concentration is changed to 15%. The heater is switched on, and the temperature is controlled at 50 °C. The cooling circulator (Deng Yng, D-620, New Taipei City, Taiwan) is switched on and the temperature for the experiment is set. When the gas inlet temperature is fixed at 50 °C, the CO_2 concentration is fixed at 15%, and the corrected pH electrode is plugged in the bubble column for operation. The initial CO_2 concentration, pH, liquid temperature, gas temperature, gas inlet pressure, and absorbent feed volume are recorded.

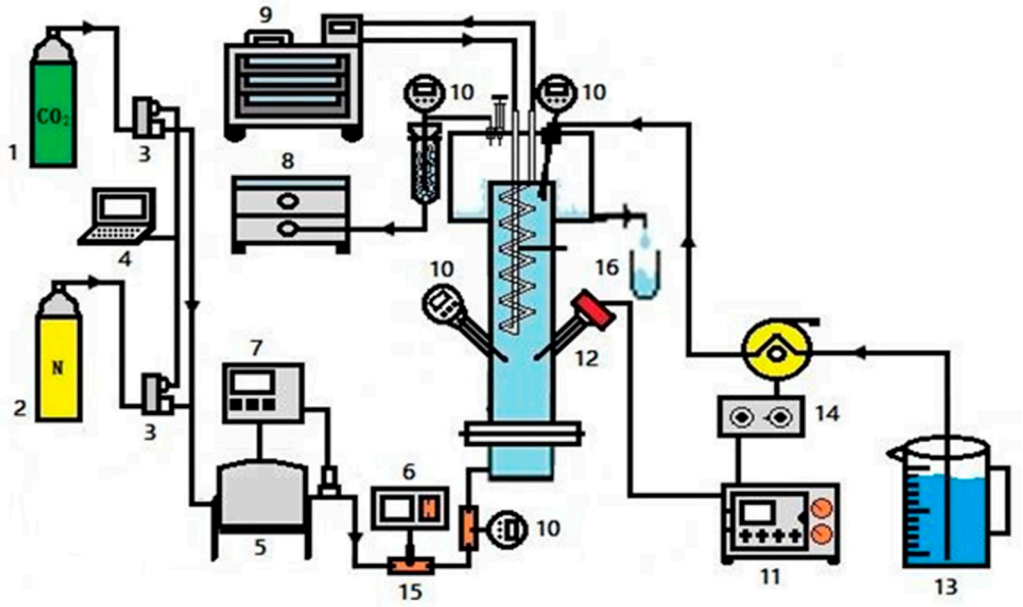

Figure 2. Schematic flow sheet for the absorption of CO_2 is explored in this study. (1) CO_2-gas tank; (2) N_2-gas tank; (3) mass flow controller; (4) PC notebook; (5) heater; (6) pressure gauge; (7) heating controller; (8) CO_2-gas meter; (9) cooling system; (10) electronic thermometer; (11) pH controller; (12) pH electrolyte; (13) storage tank; (14) tubing pump and controller; (15) reducer; (16) recovery tank.

Subsequently, the solvent is poured into the column until it overflows, and the initial solution volume in the column is recorded. The tubing pump controller (EASY-LOAD, 7518-00) and pH electrode controller are switched on for timing. As the pH decreases after the solution absorbs CO_2, the pH controller injects the sodium glycinate solution into the column automatically, so that the pH is controlled. The experimental data are recorded once every 5 min, and 10 mL of solution is taken as the sample every 10 min. When the CO_2 concentration measured by the CO_2 detector reaches a steady state, the experiment can be ended.

2.4.2. Regeneration Test

The equipment for the regeneration experiment is shown in Figure 3, including a cooling circulator, oil bath, magnetic stirrer heating plate, three-neck round flask, and a ball condenser tube. The apparatus is similar to that reported in the literature [9,37]. Firstly, 0.05 kg of solution after absorption is prepared, and the ball condenser tube, three-neck round flask, and cooling circulator are assembled. The experimental heating temperature and cooling water tank temperature (5 °C) are set. When the heating temperature and cooling circulator temperature are stable, the 0.05 kg solution is poured in and the magnetic stirrer is switched on. The experimental time is 60 min, and the temperature change is recorded once every five minutes. When the experiment is finished, the heating controller and cooling circulator are switched off, the mass of the sodium glycinate solution after the experiment is measured, and samples are taken. The samples are tested using an elements analyzer (EA) (Thermo, Flash EA1112, Cambridge, UK).

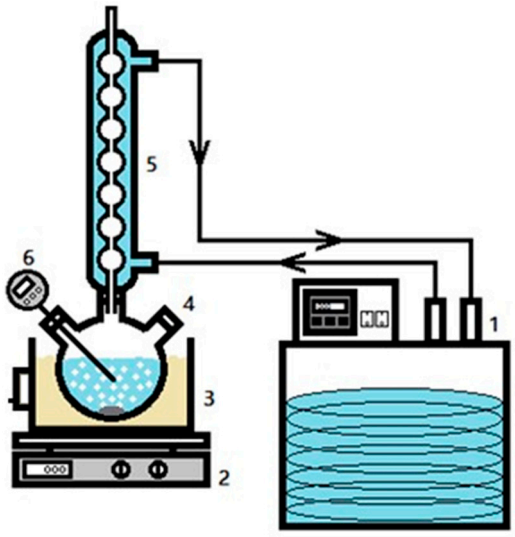

Figure 3. Schematic diagram of the apparatus used in the regeneration experiment. (1) Cooling system; (2) hot plate with stirrer; (3) oil bath; (4) three-neck round flask; (5) ball condenser tube; (6) electronic thermometer.

3. Results and Discussions

The calculated data for E, R_A, K_Ga, γ, and φ are listed in Table 5. All of the data can be analyzed to search for the optimum conditions and the importance of parameters by using the S/N ratio.

Table 5. Data obtained in the Taguchi experiments. E—absorption efficiency; R_A—absorption rate; K_Ga—overall mass transfer coefficient; γ—flow rate ratio; α—loading of CO_2.

No.	E	$R_A \times 10^4$	K_Ga	γ	Φ	α
	(%)	(mol s^{-1} L^{-1})	(s^{-1})	(-)	(mol mol^{-1} L^{-1})	(mol mol^{-1})
1	55.33	2.30	0.051	4.34	0.4079	0.5044
2	47.40	3.74	0.074	4.71	0.3892	0.4961
3	36.54	4.37	0.077	6.72	0.4339	0.5605
4	25.64	4.21	0.070	8.89	0.4028	0.6061
5	73.03	3.14	0.088	3.06	0.3845	0.3671
6	44.81	3.46	0.065	4.77	0.3727	0.4167
7	62.82	7.14	0.173	2.70	0.2995	0.3147
8	44.67	6.77	0.136	4.54	0.3448	0.4022
9	78.57	3.30	0.102	2.56	0.3513	0.3372
10	67.95	5.34	0.138	2.41	0.2887	0.2894
11	49.34	5.78	0.116	3.42	0.2902	0.3388
12	56.41	8.56	0.185	2.52	0.2512	0.2672
13	86.84	3.45	0.132	0.87	0.1298	0.1110
14	80.52	5.90	0.189	0.94	0.1326	0.1081
15	55.92	6.48	0.144	2.81	0.2707	0.2741
16	50.00	7.49	0.152	3.03	0.2604	0.2752

3.1. Effects of pH and Temperature on the Solution Composition

The effect of pH and T on the composition of solution in the scrubbed solution can be determined by ^{13}CNMR spectra, as shown in Figure 4a–d for No. 1, 5, 9, and 13, respectively. In order for a comparison, the data was adopted using the same gas flow rate, at the rate of 3 L/min, but different pHs and temperatures of the solutions we used. In Figure 4, the major peaks were presented at 42, 45, 164, 174, and 179 ppm, which shows GLY/GLH^+ at 42 ppm and 174 ppm (A', B'), $GLYH^+CO_2^-$ in 45 ppm and 179 ppm (A, B), and the HCO_3^-/CO_3^{2-} in 162 ppm (C) [37,38]. The peak at 174 ppm shifted to 179 ppm, and disappeared when the pH value increased to 11, indicating the disappearance

of carbamate, and hence an increase in the absorption of CO_2. The effect of pH on the absorption of CO_2 can be explained in E and K_Ga, as shown in Table 4; the values of E and K_Ga are 55.33 and 0.051, 73.03 and 0.088, 78.57 and 0.102, and 86.84 and 0.132 for No. 1, 5, 9, and 13, respectively. It was found that E and K_Ga increased with an increase in the pH value and T.

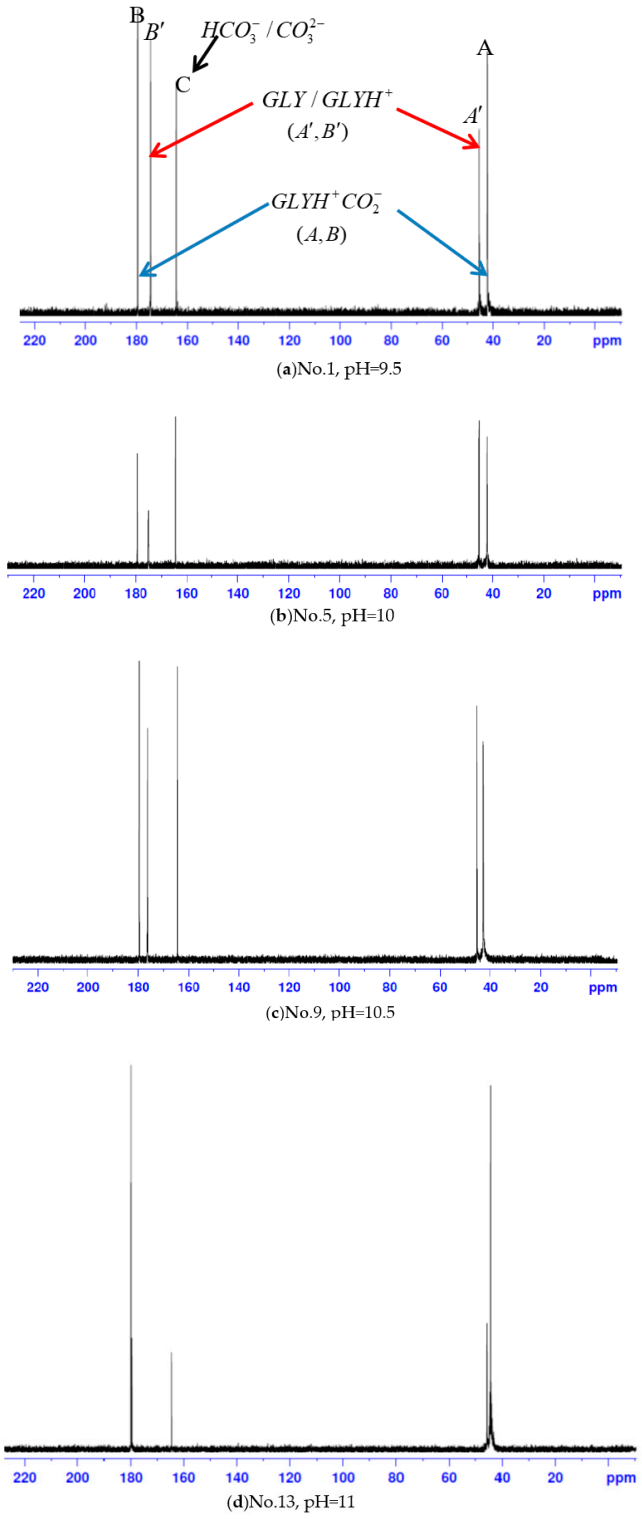

Figure 4. ^{13}CNMR spectra of sodium glycinate solution after the absorption of CO_2 gas: (**a**) No. 1; (**b**) No. 5; (**c**) No. 9; (**d**) No. 13.

3.2. Taguchi Analysis

Using an S/N ratio analysis, using data E as an example, the larger-the-better value can be determined using Equation (17). The calculated values are shown in Table 6. The results show that the importance of the parameters is B (Q_g) > A (pH) > D (C_L) > C (T), while the optimum condition is A4B1C2D1. Other analysis data, such as R_A, K_Ga, γ, and φ, can be determined using the same procedure. All of the results are collected in Table 7, showing the different results in an optimum condition and the importance of the parameters. In order to understand the importance of the parameters of the whole system, the ratios of 4, 3, 2, 1, for the sequence 1, 2, 3, and 4, respectively are set. It was found that the pH has highest rations (3.67) and T has lowest rations (1.17). Because of this, the importance of the parameters of the whole system became A > D > B > C. Figure 5 shows the importance of the parameters in a radar chart for whole system and for the individual data.

Table 6. Signal/noise (S/N) ratio analysis for absorption efficiency (E).

Level	A	B	C	D
1	31.95	37.20	33.93	35.99
2	34.81	35.33	35.19	34.79
3	35.86	34.01	35.07	34.79
4	36.46	32.55	34.89	33.52
Delta	4.51	4.65	1.26	2.47
Rank	2	1	4	3

Table 7. Optimum conditions and importance of parameters in the absorption process, according to the Taguchi analysis.

	Optimum Condition	Importance of Parameters
E	A4B1C2D1	B > A > D > C
R_A	A4B4C2D1	B > A > D > C
K_Ga	A4B4C4D1	A > D> B > C
γ (max)	A1B4C1D4	A > D > B > C
γ (min)	A4B1C4D1	A > D > B > C
φ	A1B3C1D4	A > D > C > B

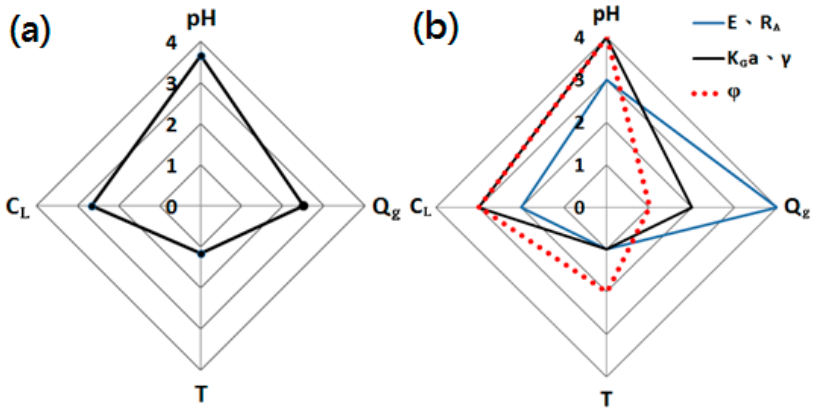

Figure 5. Significant parameters according the radar chart analysis: (**a**) whole system; (**b**) individual data.

3.3. Verification of Optimum Conditions

Verification tests of the optimum conditions were carried out using the same procedure as in the Taguchi experiment. All of the data evaluated are listed in Table 8. All of the conditions that satisfied the optimum values are shown in red. This demonstrates the feasibility and reliability of the Taguchi experimental design.

Table 8. Data obtained in the verification test of the optimum conditions.

No	Optimum Conditions	E	$R_A \times 10^4$	$K_G a$	γ	φ	α
		(%)	(mol s^{-1} L^{-1})	(s^{-1})	(-)	(mol mol^{-1} L^{-1})	(mol mol^{-1})
17	A4B1C2D1	87.01	3.53	0.132	1.00	0.1512	0.1425
18	A4B4C2D1	66.03	9.89	0.242	1.18	0.1377	0.1500
19	A4B4C4D1	73.42	11.0	0.305	0.82	0.1077	0.1093
20	A1B4C1D4	19.23	3.21	0.041	11.37	0.3864	0.5350
21	A4B1C4D1	90.26	3.64	0.152	0.74	0.1162	0.1115
22	A1B3C1D4	29.75	3.58	0.053	8.73	0.4648	0.5205

3.4. Uncontrolled Experimental Results

In order to better understand the absorption process in a pilot scale, uncontrolled experiments were carried out. Two runs were conducted here. One, for the condition of optimum E was selected (No. 17), and the other was the condition of optimum $K_G a$ (No. 19). However, pH and T were uncontrolled for both. Figure 6 shows the elapsed times in the pH and T for No. 23, while the controlled experiment (No. 17) is also presented in this figure as blue points for comparison. It was found that the change in pH was nearly the same for both of the systems, while the temperature in No. 23 was lower than in No. 17. However, the system for No. 23 reached a steady state after 40 min, which was similar to that of No. 17. Table 9 shows the data for both No. 17 and No. 23. It can be seen that the values evaluated for the controlled experiments (No. 17 and No. 19) were higher than those obtained in the uncontrolled experiments (No. 23 and No. 24). The reason for this was that the gas–liquid contact time for both were different. The contact time for the former was longer than that for the latter.

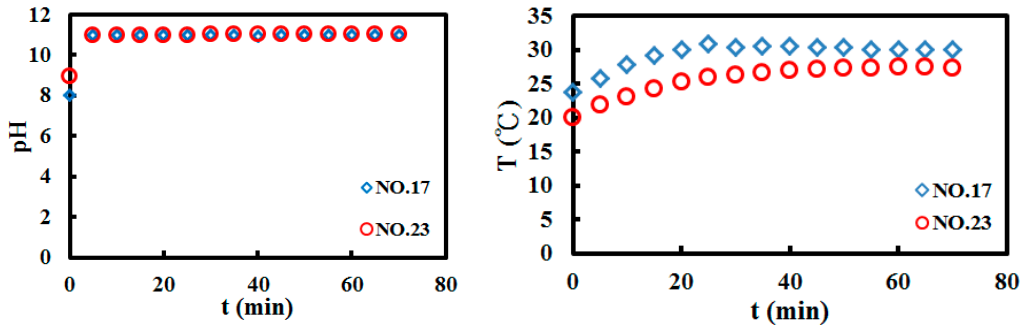

(**a**) pH vs. time (**b**) T vs. time

Figure 6. Elapsed times for pH and T for the controlled and uncontrolled experiments.

Table 9. Data evaluated and compared for both of the systems.

No.	E	$R_A \times 10^4$	$K_G a$	γ	φ	α
	(%)	(mol s^{-1} L^{-1})	(s^{-1})	(-)	(mol mol^{-1} L^{-1})	(mol mol^{-1})
17	87.01	3.53	0.132	1.00	0.1512	0.1425
23	85.90	3.52	0.125	1.00	0.1512	0.1685
19	73.42	11.0	0.305	0.82	0.1077	0.1093
24	66.23	9.75	0.243	0.82	0.0944	0.1235

3.5. Loading of CO_2 at the Final Stage

The loading of CO_2 (α) can be determined using TOC analysis (Teledyne Tekmer, Phoenix 8000, Mason, OH, USA), and the results are shown in the last column of Table 4. The obtained values are in the range of 0.1081–0.6061 mol-CO_2/mol-amine, depending on the operating conditions. It can be found that the value is related to the pH, T, and flow rate ratio (γ). The results show that the lower the pH, the higher the α value; however, it was also found that the higher the γ, the higher the α. However, the relationship between them is hard to quantitatively determine. Therefore, a linear

regression including the Taguchi experimentation is required. A total of sixteen data sets, as listed in Table 4, are adopted, and the results are shown as follows:

$$\alpha(\text{mol/mol}) = 0.3847 \exp\left(\frac{459.444}{T(\text{K})} - 0.2376\text{pH}\right)\gamma^{0.5978} \quad (19)$$

Figure 7 shows the confidence of regression, where it is found that the measured values are close to that of the calculated values, indicating that they are reliable in regression. Therefore, the equation can be used to calculate the values obtained in the optimum conditions and uncontrolled experiments. The results are also presented in Figure 7, where a slight deviation shows that Equation (19) is predicable. In addition, the parameter importance analysis shows γ > pH > T, indicating that the liquid gas contact is significant for CO_2 loading. For the sake of caparison, two solvents, MEA [35] and aqueous ammonia [36], were used in the bubble-column scrubbers for CO_2 capture, and they are also exhibited Figure 7. It was found that most of the data falls in between the error range. In addition, the loading of the aqueous ammonia was close to that obtained in this work.

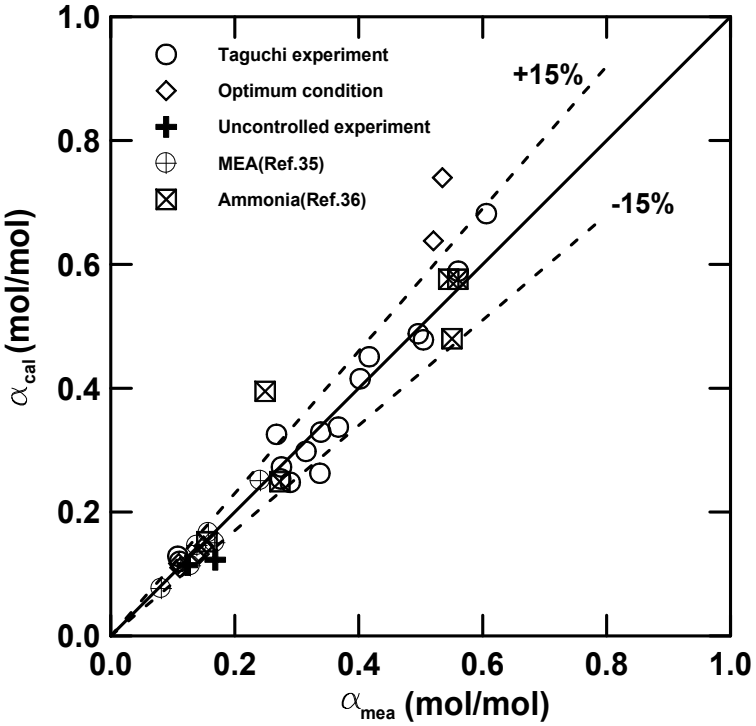

Figure 7. A plot of the calculated value versus measured values for α showing the regression confidence. MEA—monoethanolamine.

3.6. Overall Mass-Transfer Coefficient

The effects of T, pH, C_L, and Q_g on K_Ga can be found in Table 4. However, the effective correlation equation for K_Ga is not prone to being obtain. Here, the mass transfer coefficient can be correlated to the liquid molar flux, gas molar flux, and temperature [39,40]. In order to obtain the empirical equation, the gas and liquid flow rates are needed to translate into the molar flux, that is, G_x (mol/s·m^2) and G_y (mol/s·m^2); the values are in the range of 0.9469–2.8407 mol/s·m^2 and 0.2321–1.7936 mol/s·m^2 for G_y and G_x, respectively. Using the linear regression, a total of sixty data sets for K_Ga, as listed in Table 4, were used. The correlation results became the following:

$$K_Ga(1/\text{s}) = 1.2525 \exp\left(-\frac{661.062}{T(\text{K})}\right)[G_x(\text{mols}^{-1}\text{m}^{-2})]^{0.6069}[G_y(\text{mols}^{-1}\text{m}^{-2})]^{0.08109} \quad (20)$$

In order to understand the confidence of regression, a plot of $(K_G a)_{cal}$ versus $(K_G a)_{mea}$ is shown in Figure 8, where it is found that the most data are within a 15% error and are close to the solid line, indicating that regression is reasonable. In order to verify the optimum experiments and the uncontrolled experiments, all of the data were plotted in the figure. It was found that all of the data are close to the solid line, thus, Equation (20) is reliable. In addition, from an operation range analysis, the parameter importance was found to be $G_x > T > G_y$. Because of this, controlling G_x can effectively improve the $K_G a$. This could be done by increasing the pH of the solution. In addition, the $K_G a$ values obtained in the two solvents, MEA [35] and aqueous ammonia [36], which were used in the bubble-column scrubbers for CO_2 absorption, were shown in the same figure for comparison. It was found that the reported data for the two solvents were close to that obtained in this work. This indicated that the $K_G a$ of a sodium glycinate solution is comparable to that of the MEA and aqueous ammonia solvents. The range in $K_G a$ for the three solvents was 0.04–0.4 s^{-1}, depending on the operating conditions.

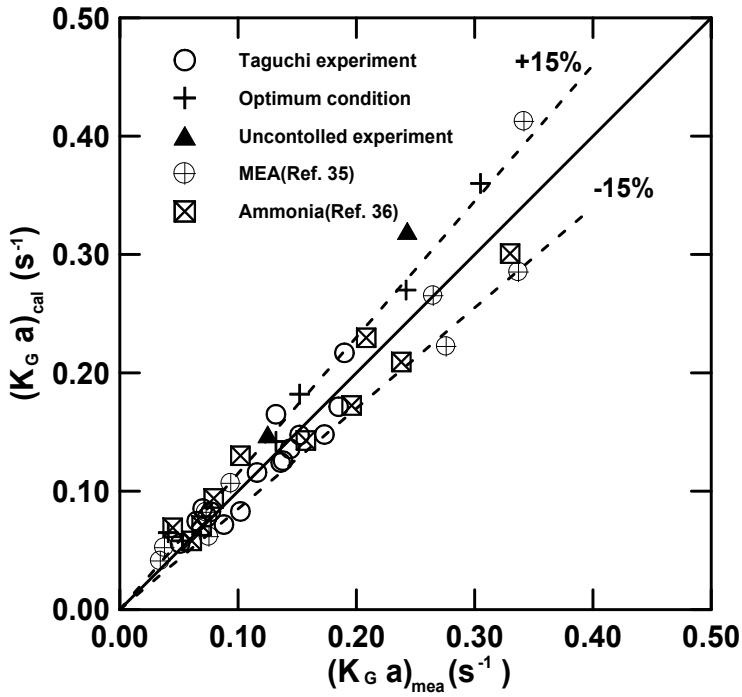

Figure 8. A plot of the calculated value versus measured values for $K_G a$ showing the regression confidence.

3.7. Heat of Regeneration of CO_2 Loaded Sodium Glycinate Solution

The regeneration energy can be determined by the thermal data and energy balance, as shown in Equation (13), and the results are listed in Table 10 and Figure 9. It was found that the individual penalties were 0.181–0.453 GJ t^{-1}, 1.66–4.38 GJ t^{-1}, and 0.51–7.43 GJ t^{-1} for Q_{abs}, Q_{sen}, and Q_{sol}, respectively. Therefore, the total energy required here was in the range of 3.68–10.75 GJ t^{-1}, which is higher than 5.0 GJ/t, comparable to that reported by Rabensteiner et al. [22]. From the energy duty distribution analysis, it can be found that the heat of absorption is below 5%, while the heat of evaporation and the sensitive heat are both close to 48%. Therefore, a reduction in Q_{sen} and Q_{sol} can effectively obtain a small Q.

Table 10. Heat of regeneration for different conditions.

Condition	No.	T_R	Q_{abs}	Q_{sen}	Q_{sol}	Q
		(°C)	(GJ t^{-1})	(GJ t^{-1})	(GJ t^{-1})	(GJ t^{-1})
No. 17	R1	100	0.225	3.02	3.11	6.35
	R2	110	0.216	2.95	4.40	7.56
	R3	120	0.208	2.77	6.96	9.94
No. 18	R4	100	0.231	3.55	4.07	7.85
	R5	110	0.222	2.70	2.76	5.68
	R6	120	0.214	2.64	6.61	9.46
No. 19	R7	100	0.186	2.99	0.51	3.68
	R8	110	0.188	2.76	2.12	5.07
	R9	120	0.181	2.74	4.16	7.08
No. 20	R10	100	0.453	3.55	0.53	4.55
	R11	110	0.435	2.23	3.07	5.74
	R12	120	0.418	1.66	4.07	6.15
No. 21	R13	100	0.197	4.13	3.53	7.85
	R14	110	0.188	3.48	1.15	4.81
	R15	120	0.181	2.88	2.57	5.63
No. 22	R16	100	0.446	3.17	2.32	5.93
	R17	110	0.428	4.38	4.54	9.34
	R18	120	0.412	2.91	7.43	10.75

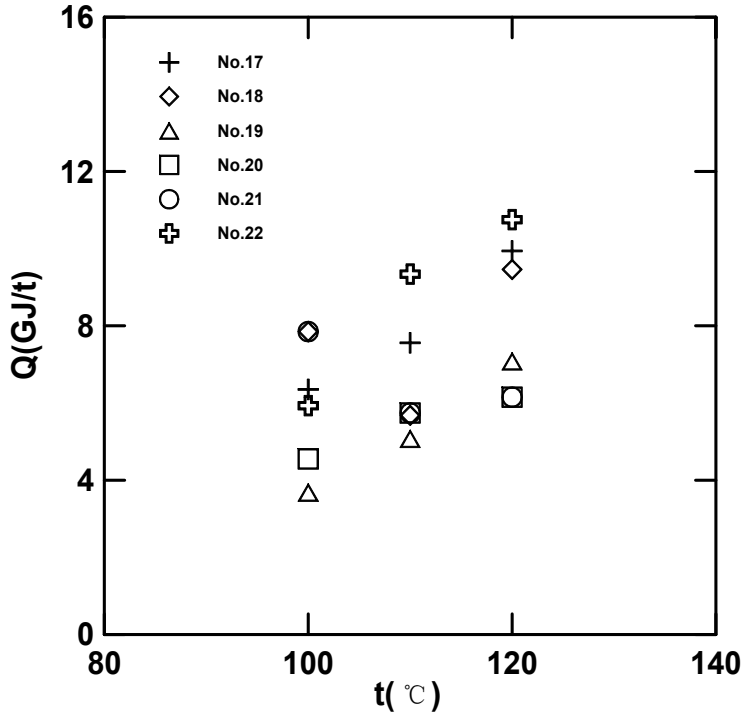

Figure 9. Heat of regeneration as a function of loading and regeneration temperature.

However, the heat of regeneration can be correlated with the pH of the solution, regeneration temperature, and CO_2 loading. A total of eighteen data was adopted for regression as shown below:

$$Q(\mathrm{GJ/t}) = 0.5110 \exp(0.9343\mathrm{pH} - \frac{2158.9}{T_R(\mathrm{K})})\alpha^{1.002} \quad (21)$$

It can be found that most of the data in Figure 10 shows a ±20% error. Equation (21) can be used to predict the heat of regeneration when the loading, temperature, and pH of the solution are given. In addition, the analysis showed that the sequence of the parameter is α > pH > T_R, indicating the importance of CO_2 loading. This implies that the loading control is important for reducing the heat of regeneration. In addition, in the real stripper, the efficiency could be higher, as the gas–liquid contact environment is better and the effect of pressure on the CO_2 stripping could be obviously.

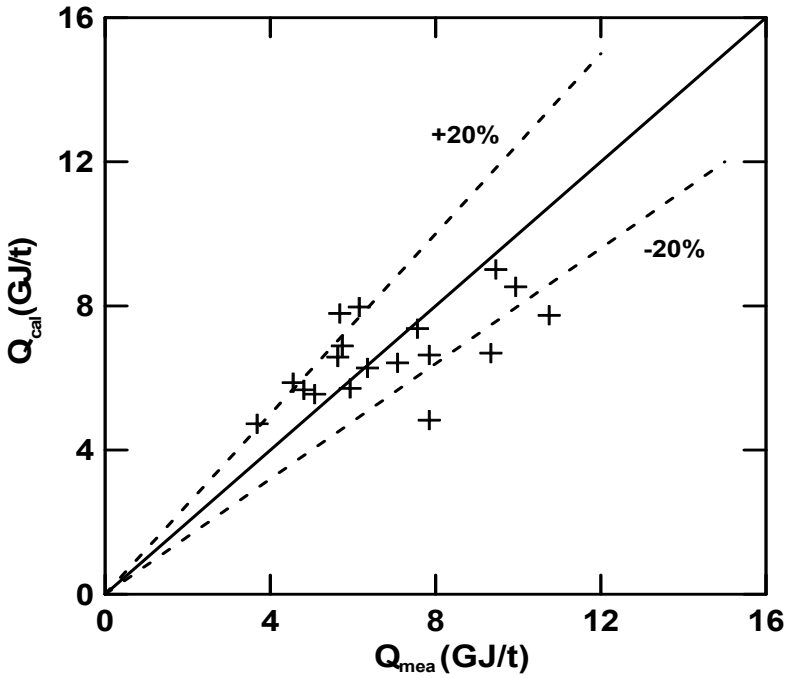

Figure 10. A plot of Q_{cal} versus Q_{mea} showing the confidence of regression.

3.8. Operating Policy

From the uncontrolled experiments, the operating pH and liquid temperature (T) are around 11 and 28 °C, respectively, after steady-state operation. The K_Ga and E values for No. 23 and No. 24, shown in Table 9, are 85.90 and 0.125, and 66.23 and 0.243, respectively. The different E and K_Ga values for the two runs are due to differences in G_x and G_y, which are 1.03 and 1 for No. 23, and 3.66 and 3 for No. 24, respectively. This indicates that at a higher mixing intensity, No. 24 has a higher K_Ga, but reduces its removal efficiency. From the designation viewpoint, a higher K_Ga has a smaller size, and hence gets more effective in the removal of CO_2. If we assume the removal efficiency E = 80%, the K_Ga becomes 0.16 s^{-1}, which falls in between the two values. In this manner, the evaluated α is 0.1123, using Equation (19), and the Q is 5.08 GJ/t, using Equation (21), at T_R = 373K. Therefore, a mild mixing and increase in the pH of the solution are required to give a higher K_Ga and a higher E. Alternatively, an agitator put inside the column could enhance the dispersion and mixing, which makes K_Ga and E higher.

4. Conclusions

This study successfully used a continuous bubble-column scrubber with a sodium glycinate solution to capture CO_2. Using material balance with a two-film model, the absorption rate, overall mass-transfer coefficient, CO_2 loading, and scrubbing factor could be determined at a steady-state condition. Quantitatively, the effects of the variables on the E, K_Ga, R_A, γ, α, and φ can be explained using the empirical equations obtained by this study. The operating range for γ was found to be in the range of 0.74–11.37, which is flexible. The heat of the regeneration (Q) mechanism analysis suggests that a reduction of the evaporation heat and sensitive heat can obviously attenuate the Q in a

stripper. The ^{13}CNMR spectra of the scrubbed solution for the glycine system showed GLY/$GLYH^+$, $GLYH^+CO_2^-$, and HCO_3^-/CO_3^{2-}, depending on the absorption conditions. At a higher pH, it favors E and K_Ga, but reduces the values of γ, while α and φ show the pH on the effect of the solution chemistry. E and K_Ga can reach 80% and 0.16 s^{-1}, respectively; when $\gamma < 1$, it corresponds to a pH of 11. In this manner, α is less than 0.12 mol/mol, which can reduce the Q value. The regression equations in K_Ga, α, and Q can satisfy the optimum conditions and uncontrolled experiments. Because of this, empirical equations can be used to predict the K_Ga, α, and Q for a pilot-scale bubble-column scrubber and heat regeneration. Finally, the order of parameter importance is pH > C_L > Q_g > T, which can be effectively adjusted in order to obtain the desired E, K_Ga, and α within the operating range in this work.

Author Contributions: P.C.C. conceived and designed the experiments and wrote the paper, while S.-Z.L. performed the experiments and analyzed the data.

Funding: The funding was supported by the Ministry of Science and Technology, Taiwan, ROC.

Acknowledgments: The authors acknowledge the financial support of the MOST in Taiwan ROC (MOST-104-2221-E-262-012).

Conflicts of Interest: The authors declare no conflicts of interest.

Abbreviations

EA	element analysis
MEA	monoethanolamine
NMR	nuclear magnetic resonance
SG	sodium glycinate
S/N	signal/noise

Nomenclature

C_L	[mol/L]	concentration of sodium glycinate (SG) in liquid phase
C_g	[mol/L]	concentration of CO_2 in the gas phase
C_p	[J/kg·k]	heat capacity of liquid
E	[%]	removal efficiency
F_{A1}	[mol/s]	molar flow rate of CO_2 at inlet
F_{A2}	[mol/s]	molar flow rate of CO_2 at outlet
F_L	[mol/s]	molar flow rate of SG solution at inlet
F_G	[mol/s]	molar flow rate of gas at inlet
H	[-]	Henry's constant
ΔH_{abs}	[kJ/kg]	heat of absorption
ΔH_{vap}	[kJ/kg]	heat of evaporation
K_Ga	[1/s]	overall mass-transfer coefficient
$(K_Ga)_{loc}$	[1/s]	local overall mass-transfer coefficient
L_i	[-]	number of level of ith variable
m_{sol}	[kg]	the mass of regeneration solution
Δm_1	[kg]	the solvent loss of CO_2 after stripping
Δm	[kg]	the mass loss of during stripping
n	[-]	total number of required runs
P	[pa]	pressure
P_1	[pa]	pressure at inlet
P_2	[pa]	pressure at outlet
Q	[GJ/t]	heat duty of solvent regeneration
Q_{abs}	[GJ/t]	heat of absorption
$\dot{Q}_C$	[J/min]	cooling rate
Q_g	[L/min]	gas volumetric flow rate

Q_L	[L/min]	liquid flow rate
Q_{sen}	[GJ/t]	sensitive heat of solution
Q_{sol}	[GJ/t]	heat of evaporation
R	[-]	gas–liquid flow rate ratio
R_A	[mol/s·L]	absorption rate
V	[L]	volume of bubble column
V_L	[L]	volume of liquid in bubble column
S/N	[-]	mean signal-to-noise ratios
t_1	[sec]	evaporation time
T	[°C]	temperature
T_1	[K]	absolute temperature at inlet
T_2	[K]	absolute temperature at outlet
T_R	[K]	regeneration temperature
y_1	[-]	more fraction of CO_2 at inlet
y_2	[-]	mole fraction of CO_2 at outlet
z_i	[-]	the measured data for *i*th run
α	[mol/mol]	loading
γ	[-]	gas–liquid molar flow rate ratio
φ	[mol·CO_2/L·mol·SG]	scrubbing factor
ω	[-]	weight fraction of SG

References

1. Yang, H.; Xu, Z.; Fan, M.; Gupta, R.; Slimane, R.B.; Bland, A.E.; Wright, I. Progress in carbon dioxide separation and capture: A review. *J. Environ. Sci.* **2008**, *20*, 14–27. [CrossRef]
2. Chen, P.C.; Shi, W.; Du, R.; Chen, V. Scrubbing of CO_2 greenhouse gases, accompanied by precipitation in a continuous bubble-column Scrubber. *Ind. Eng. Chem. Res.* **2008**, *47*, 6336–6343. [CrossRef]
3. Yu, C.H.; Huang, C.H.; Tan, C.S. A review of CO_2 capture by absorption and adsorption. *Aerosol Air Qual. Res.* **2012**, *12*, 745–769. [CrossRef]
4. Han, K.; Ahn, C.K.; Lee, M.S. Performance of an ammonia-based CO_2 capture pilot facility in iron and steel industry. *Int. J. Greenh. Gas Control* **2014**, *27*, 239–246. [CrossRef]
5. Mondal, M.P.; Guha, M.; Biswas, A.K.; Bandyopadhyay, S.S. Removal of carbon dioxide by absorption in mixed amines: Modelling of absorption in aqueous MDEA/MEA and AMP/MEA solutions. *Chem. Eng. Sci.* **2001**, *56*, 6217–6224. [CrossRef]
6. Idem, R.; Wilson, M.; Tontiwachwuthikul, P.; Chakma, A.; Veawab, A.; Aroonwilas, A.; Gelowitz, D. Pilot plant studies of the CO_2 capture performance of aqueous MEA and Mixed MEA/MDEA solvents at the University of Regina CO_2 capture technology development plant and boundary dam CO_2 capture demonstration plant. *Ind. Eng. Chem. Res.* **2006**, *45*, 2414–2420. [CrossRef]
7. Fu, D.; Lin, W.; Liu, S.T. Experiment and model for the surface tension of carbonated MEA-MDEA aqueous solutions. *Fluid Phase Equilib.* **2013**, *337*, 83–88. [CrossRef]
8. Li, T.; Keener, T.C. A review: Desorption of CO_2 from rich solutions in chemical absorption processes. *Int. J. Greenh. Gas Control* **2016**, *51*, 290–304. [CrossRef]
9. Lin, P.H.; Wong, D.S.H. Carbon dioxide capture and regeneration with amine/alcohol/water blends. *Int. J. Greenh. Gas Control* **2014**, *26*, 69–75. [CrossRef]
10. De Avila, S.G.; Logli, M.A.; Matos, J.R. Kinetic study of the thermal decomposition of monoethanolamine (MEA), diethanolamine (DEA), triethanolamine (TEA) and methyldiethanolamine (MDEA). *Int. J. Greenh. Gas Control* **2015**, *42*, 666–671. [CrossRef]
11. Wu, S.H.; Caparanga, A.R.; Leron, R.B.; Li, M.H. Vapor pressures of aqueous blended-amine solutions containing (TEA/AMP/MDEA)+(DEA/MEA/PZ) at temperatures (303.15–343.15) K. *Exp. Therm. Fluid Sci.* **2013**, *48*, 1–7. [CrossRef]
12. Ali Khan, A.; Halder, G.N.; Saha, A.K. Carbon dioxide capture characteristics from flue gas using aqueous 2-amino-2-methyl-1-propanal (AMP) and monoethanolamine (MEA) solutions in packed bed absorption and regeneration columns. *Int. J. Greenh. Gas Control* **2015**, *32*, 15–23. [CrossRef]

13. Oyenekan, B.A.; Rochelle, G.T. Energy performance of stripper configurations for CO_2 capture by aqueous amines. *Ind. Eng. Chem. Res.* **2006**, *45*, 2457–2464. [CrossRef]
14. Rinprasertmeechai, S.; Chavadej, S.; Rangsunvigit, P.; Kulprathipanja, S. Carbon dioxide removal from flue gas using amine-based hybrid solvent absorption. *Int. J. Chem. Mol. Nucl. Mater. Metall. Eng.* **2012**, *6*, 284–288.
15. Yan, S.; He, Q.; Ai, P.; Wang, Y.; Zhang, Y. Regeneration performance of concentrated CO_2-rich alkanolamine solvents: The first step study of a novel concept for reducing regeneration heat consumption by using concentration swing absorption technology. *Chem. Eng. Process* **2013**, *70*, 86–94. [CrossRef]
16. Chen, P.C.; Yang, M.W.; Wei, C.H.; Lin, S.Z. Selection of blended amine for CO_2 capture in a packed bed scrubber using the Taguchi method. *Int. J. Greenh. Gas Control* **2016**, *45*, 245–252. [CrossRef]
17. Oyenekan, B.A.; Rochelle, G.T. Alternative stripper configurations for CO_2 capture by aqueous amines. *AIChE J.* **2007**, *53*, 3144–3154. [CrossRef]
18. Park, S.W.; Son, Y.S.; Park, D.W.; Oh, K.J. Absorption of Carbon Dioxide into Aqueous. Solution of Sodium Glycinate. *Sep. Sci. Technol.* **2008**, *43*, 3003–3019. [CrossRef]
19. Guo, B.S.; Jing, G.H.; Zhou, Z.M. Regeneration performance and absorption/desorption mechanism of tetramethylammonium glycinate aqueous solution for carbon dioxide. *Int. J. Greenh. Gas Control* **2015**, *34*, 31–38. [CrossRef]
20. Weiland, H.; Hatcher, N.A.; Nava, J.L. Benchmarking Solvents for Carbon Capture. *Process. Distill. Absorpt.* **2010**, 139–144.
21. Vaidya, P.D.; Konduru, P.; Vaidyanathan, M. Kinetics of carbon dioxide removal by aqueous alkaline amino acid salts. *Ind. Eng. Chem. Res.* **2010**, *49*, 11067–11072. [CrossRef]
22. Rabensteiner, M.; Kinger, G.; Koller, M.; Gronald, G.; Unterberger, S.; Hochenauer, C. Investigation of the suitability of aqueous sodium glycinate as a solvent for post combustion carbon dioxide capture on the basis of pilot plant studies and screening methods. *Int. J. Greenh. Gas Control* **2014**, *29*, 1–15. [CrossRef]
23. Aronu, U.E.; Svendsen, H.F.; Hoff, K.A. Investigation of amine amino acid salts for carbon dioxide absorption. *Int. J. Greenh. Gas Control* **2010**, *4*, 771–775. [CrossRef]
24. Kumar, P.S.; Hogendoorn, J.A.; Versteeg, G.F.; PFeron, P.H.M. Kinetics of the reaction of CO_2 with aqueous potassium salt of taurine and glycine. *AIChE J.* **2003**, *49*, 203–213. [CrossRef]
25. Portugal, A.F.; Derks, P.W.J.; Versteeg, G.F.; Magalhaes, F.D.; Mendes, A. Characterization of potasium glycinate for carbon dioxide absorption purposes. *Chem. Eng. Sci.* **2007**, *62*, 6534–6547. [CrossRef]
26. Lee, S.; Song, H.J.; Maken, S.; Park, J.W. Kinetics of CO_2 absorption in aqueous sodium glycinate solutions. *Ind. Eng. Chem. Res.* **2007**, *46*, 1578–1583. [CrossRef]
27. Park, S.J.; Jang, K.R.; Park, I.H. Determination and calculation of physical properties for sodium glycinate as a CO_2 absorption. *Korean Chem. Eng. Res.* **2006**, *44*, 277–283.
28. Song, H.J.; Lee, S.; Maken, S.; Park, J.J.; Park, J.W. Solubilities of carbon dioxide in aqueous solutions of sodium glycinate. *Fluid Phase Equilib.* **2006**, *246*, 1–5. [CrossRef]
29. Salazar, V.; Sánchez-Vicente, Y.; Pando, C.; Renuncio, J.A.R.; Cabanas, A. Enthalpies of Absorption of Carbon Dioxide in Aqueous Sodium Glycinate Solutions at Temperatures of (313.15 and 323.15) K. *J. Chem. Eng. Data* **2010**, *55*, 1215–1218. [CrossRef]
30. Shaikh, M.S.; Shariff, A.M.; Bustam, M.A.; Murshid, G. Analysis of physicochemical properties of aqueous sodium glycinate (SG) solution at law concentrations form 0.1–2.0 M. *J. Appl. Sci.* **2014**, *14*, 1055–1060. [CrossRef]
31. Vandu, C.O.; Koop, K.; Krishna, R. Volumetric mass transfer coefficient in a slurry bubble column operating in the heterogeneous flow regime. *Chem. Eng. Sci.* **2004**, *59*, 5417–5423. [CrossRef]
32. Dhaouadi, H.; Poncin, S.; Hornut, J.M.; Midoux, N. Gas-liquid mass transfer in bubble column reactor: Analytical solution and experimental confirmation. *Chem. Eng. Process.* **2008**, *47*, 548–556. [CrossRef]
33. Lau, R.; Lee, P.H.V.; Chen, T. Mass transfer studies in shallow bubble column reactors. *Chem. Eng. Process.* **2012**, *62*, 18–25. [CrossRef]
34. Al-Naimi, S.A.; Salih, S.A.J.; Mohsin, H.A. Simulation study of mass transfer coefficient in slurry bubble column reactor using neural network. *Al-Khwarizmi Eng. J.* **2013**, *9*, 60–70.
35. Chen, P.C.; Luo, Y.X.; Cai, P.W. Capture of carbon dioxide using monoethanolamine in a bubble-column scrubber. *Chem. Eng. Technol.* **2015**, *38*, 274–282. [CrossRef]

36. Chen, P.C.; Yu, S.C. CO_2 capture and crystallization of ammonia bicarbonate in a lab-scale scrubber. *Crystals* **2018**, *8*, 39. [CrossRef]
37. Song, H.J.; Lee, S.; Park, K.; Lee, J.; Filburn, T.P. Simplified Estimation of Regeneration Energy of 30 wt % Sodium Glycinate Solution for Carbon Dioxide Absorption. *Ind. Eng. Chem. Res.* **2008**, *47*, 9925–9930. [CrossRef]
38. Ciftja, A.F.; Hartono, A.; Svendsen, H.F. Selection of amine amino acids salt systems for CO_2 capture. *Energy Procedia* **2013**, *37*, 1597–1604. [CrossRef]
39. McCabe, W.L.; Smith, J.C.; Harriot, P. *Unit Operation of Chemical Engineering*, 5th ed.; McGraw-Hill, Inc.: New York, NY, USA, 1993.
40. Remacha, N.; Jose, M.; Kulkarni, A.A.; Jensen, K.F. Gas-liquid flow and mass transfer in an advanced-flow reactor. *Ind. Eng. Chem. Res.* **2013**, *52*, 8996–9010. [CrossRef]